Journal of Power Sources 196 (2011) 6710–6715

Contents lists available at ScienceDirect

Journal of Power Sources

journal homepage: www.elsevier.com/locate/jpowsour

Effects of manganese and cobalt on the electrochemical and thermal properties of layered $Li[Ni_{0.52}Co_{0.16+x}Mn_{0.32-x}]O_2$ cathode materials

Hyoung-Geun Kim[a,c], Seung-Taek Myung[b,*], Jung Kyu Lee[d], Yang-Kook Sun[a,c,**]

[a] Department of WCU Energy Engineering, Hanyang University, Seoul 133-791, South Korea
[b] Department of Chemical Engineering, Iwate University, 4-3-5 Ueda, Morioka, Iwate 020-8551, Japan
[c] Department of Chemical Engineering, Hanyang University, Seoul 133-791, South Korea
[d] Department of Chemical Engineering, Dong-A University, Pusan 604-714, South Korea

ARTICLE INFO

Article history:
Received 27 August 2010
Received in revised form 5 November 2010
Accepted 8 November 2010
Available online 13 November 2010

Keywords:
Coprecipitation
Stability
Interfacial resistance
Cathode
Lithium battery

ABSTRACT

We investigate the effects of the Co and Mn ratio on the structure, morphology, electrochemical properties, and thermal stability of $Li[Ni_{0.52}Co_{0.16+x}Mn_{0.32-x}]O_2$ cathode materials. $Li[Ni_{0.52}Co_{0.16+x}Mn_{0.32-x}]O_2$ ($x = 0$, 0.08, 0.16) cathode materials are prepared via high temperature calcination of LiOH and coprecipitated $[Ni_{0.52}Co_{0.16+x}Mn_{0.32-x}](OH)_2$ hydroxides. From an X-ray diffraction investigation, the prepared materials have a well ordered O_3 type α-$NaFeO_2$ layer structure ($R\bar{3}m$). As the Co content (x) is increased, the initial discharge capacity increase slightly but it is accompanied by severe capacity fading during extensive cycling. Meanwhile, a small increase of Mn enhances the electrochemical stability at high temperature (55 °C) as well as the thermal stability. Electrochemical impedance spectroscopy reveals that manganese substitution is effective to reduce the resistance during cycling due to stabilization of the host structure.

1. Introduction

Lithium-ion batteries have become the state-of-the-art power source for electronic devices including laptop computers, cellular phones, and digital cameras. Even more important is the realization of high capacity batteries for hybrid and electric vehicles. In order to achieve this goal, the electrochemical properties of electrode active materials in addition to lower cost, longer cycle life, and better safety characteristics should be improved.

Over the past several years, layered Ni-rich $Li[Ni_{1-x}M_x]O_2$ (M = metal) materials have been intensively studied as an alternative cathode material for rechargeable lithium-ion batteries to replace lithium cobalt oxide ($LiCoO_2$) due to its drawbacks including toxicity, high cost, and instability at higher potentials (≥4.3 V vs. Li) [1,2]. Compared to $LiCoO_2$, Ni-rich $Li[Ni_{1-x}M_x]O_2$ has a large reversible capacity of approximately 200 mAh g^{-1} in the voltage range of 2.0–4.3 V vs. Li. However, Ni-rich $Li[Ni_{1-x}M_x]O_2$ has also disadvantages such as poor thermal stability and poor cycle life.

To improve the electrochemical properties of Ni-rich $Li[Ni_{1-x}M_x]O_2$, partial substitution of Ni with other metals has been performed. In particular, substitution of Co and Mn for Ni in $Li[Ni_{1-x-y}Co_xMn_y]O_2$ has resulted in substantially improved electrochemical properties and thermal stability without sacrificing the discharge capacity due to complete formation of a solid solution [3–6]. The capacity and thermal stability of layered $Li[Ni_{1-x-y}Co_xMn_y]O_2$ cathodes seem to be strongly dependent on the Co and Mn contents. Based on our previous report, the presence of tetravalent Mn in the structure leads to not only good electrochemical properties but also improved thermal stability [7].

For this reason, we investigated the effect of the Mn content on the electrochemical properties and thermal stability of $Li[Ni_{0.52}Co_{0.16+x}Mn_{0.32-x}]O_2$ ($x = 0$, 0.08, and 0.16) cathode materials for application in secondary lithium-ion batteries.

2. Experimental

Spherical $Li[Ni_{0.52}Co_{0.16+x}Mn_{0.32-x}]O_2$ ($x = 0$, 0.08, and 0.16) powders with various metal compositions ($Li[Ni_{0.52}Co_{0.16}Mn_{0.32}]O_2$, $Li[Ni_{0.52}Co_{0.24}Mn_{0.24}]O_2$, and $Li[Ni_{0.52}Co_{0.32}Mn_{0.16}]O_2$) were prepared via a co-precipitation method [8]. An aqueous solution of M (M = $NiSO_4{\cdot}6H_2O$, $CoSO_4{\cdot}7H_2O$, and $MnSO_4{\cdot}5H_2O$) was pumped into a continuous stirred tank reactor (CSTR, capacity of 4 L) under a N_2 atmosphere. At the same time, a NaOH solution (aq) and a NH_4OH solution (aq) as a chelating agent were also separately fed into the reactor. The reactor temperature was maintained at 50 °C for 20 h while closely monitoring and controlling the concentration, pH, temperature, and stirring

* Corresponding author. Tel.: +81 19 621 6345; fax: +81 19 621 6345.
** Corresponding author. Tel.: +82 2 2220 0524; fax: +82 2 2282 7329.
E-mail addresses: smyung@iwate-u.ac.jp (S.-T. Myung), yksun@hanyang.ac.kr (Y.-K. Sun).

0378-7753/$ – see front matter © 2010 Elsevier B.V. All rights reserved.
doi:10.1016/j.jpowsour.2010.11.045

speed of the mixture during the reaction process. The obtained $[Ni_{0.52}Co_{0.16+x}Mn_{0.32-x}](OH)_2$ powders were filtered, washed, and vacuum dried at room temperature. Finally, the prepared hydroxides were mixed with LiOH and then calcined at 820 °C for 15 h in air. The chemical compositions of the synthesized materials were determined by atomic absorption spectroscopy (AAS, Vario 6, Analyticjena).

Powder X-ray diffraction (XRD, Rint-2000, Rigaku, Japan) using Cu-Kα radiation was applied to identify the crystal structure of the synthesized material. The FULLPROF Rietveld program was applied to analyze the powder diffraction patterns [9]. The morphologies of the as-prepared powders were observed using a scanning electron microscope (SEM, JSM 6400, JEOL, Japan).

The cathodes were fabricated using a mixture of prepared powders (85 wt.%), carbon black (7.5 wt.%), and polyvinlylidene fluoride in *N*-methyl-2-pyrrolidinon (7.5 wt.%). The slurry was applied on Al foil and dried in an oven at 110 °C. The electrode was roll-pressed and then dried at 120 °C overnight under vacuum prior to use. The electrochemical properties were tested by using coin-type R2032 cells with lithium metal negative and counter electrodes. The electrolyte solution was 1 M $LiPF_6$ in a 1:1 volume mixture of ethylene carbonate and diethyl carbonate (PANAX ETEC Co. Ltd., Korea). The cell assembly was carried out in an Ar-filled glove box.

Differential scanning calorimetry (DSC) experiments were carried out with the cathodes by fully charging the cells to 4.5 V versus Li and opening them in the Ar-filled dry box. After carefully opening the cell in the Ar-filled dry box, the measurements were carried out in a Pyris 1 Differential Scanning Calorimeter (NETZSCH-TA4, Germany) at a temperature scan rate of 5 °C min^{-1} in the temperature range of 50–400 °C.

AC impedance measurements were performed using a Zahner Elektrik IM6 impedance analyzer over the frequency range of 5 mHz–5 MHz with an ac amplitude of 10 mV.

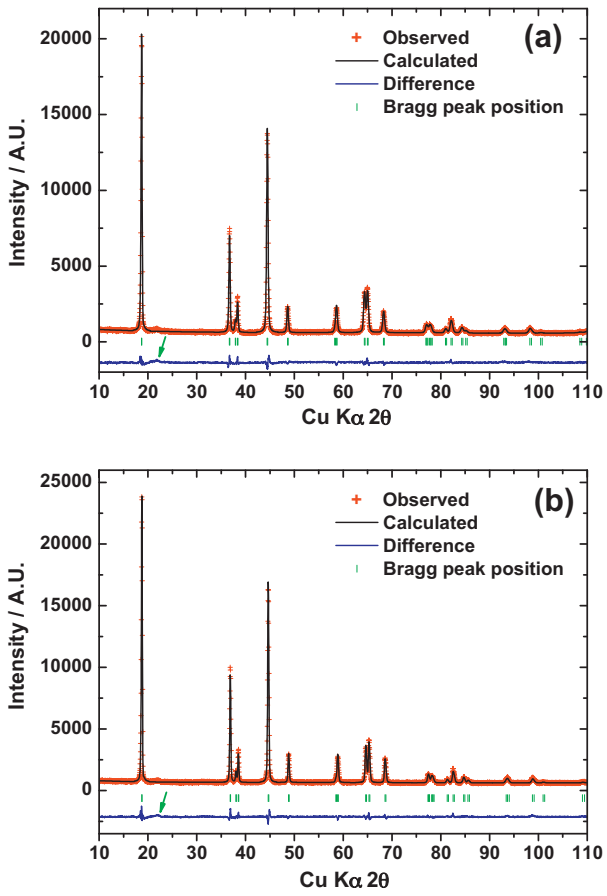

Fig. 1. Rietveld refinement result of XRD patterns of the as-synthesized (a) $Li[Ni_{0.52}Co_{0.16}Mn_{0.32}]O_2$ and (b) $Li[Ni_{0.52}Co_{0.32}Mn_{0.16}]O_2$ powders.

3. Results and discussion

Fig. 1 shows the Rietveld refinement results of the XRD patterns of the as-synthesized $Li[Ni_{0.52}Co_{0.16}Mn_{0.32}]O_2$ (Table 1) and $Li[Ni_{0.52}Co_{0.32}Mn_{0.16}]O_2$ powders. All peaks were indexed based on a hexagonal α-$NaFeO_2$ structure with a space group of $R\bar{3}m$. The splits of the (0 0 6)/(1 0 2) and (1 0 8)/(1 1 0) pairs for all samples indicate the formation of a layer structure. Interestingly, the splitting became sharper and the diffraction peaks moved to a higher angle with reduced Mn content, indicating lattice shrinkage by Co incorporation [10]. This characteristic results from the intrinsic properties of $LiCoO_2$, which exhibits a complete peak separation of the (1 0 8) and (1 1 0) peaks [11]. The AAS analysis reveals that the metal compositions of the obtained $Li[Ni_{0.52}Co_{0.16+x}Mn_{0.32-x}]O_2$ powder (x = 0–0.16) samples are similar to that of the starting composition, implying that the designated products were synthesized.

As seen in the XRD patterns in Fig. 1a and b, a small peak appeared at around 22° (2θ), indicative of a superstructure stemming from Ni^{2+} and Mn^{4+} arrangements in the oxide lattice. Thus, site exchange between Li and transition metal layers for both elements was allowed for the Rietveld refinement because the ionic radii of Li^+ (0.76 Å) and Ni^{2+} (0.69 Å) [12] are similar. The refinements resulted in good agreement between the observed and calculated patterns, which indicates that Co^{3+} and Mn^{4+} elements were incorporated into the transition metal layer, as expected. Furthermore, the resulting *a*- and *c*-axes monotonously decreased with increasing Mn content, as seen in Fig. 6. These phenomena result from the difference in the ionic radii of Ni^{2+} (0.69 Å), Co^{3+} (0.545 Å), and Mn^{4+} (0.53 Å) [12]. As described in Table 2, the divalent Ni content was also increased by decreasing trivalent Co and increasing tetravalent Mn in the transition metal layer. This result is mainly due to the decreased amount of Co because $LiCoO_2$ has a much lower occupation of Co^{3+} in the Li layer due to the difference in the ionic radii of Li^+ and Co^{3+}. Meanwhile, $Li[Ni_{0.5}Mn_{0.5}]O_2$, of which the valences of Ni and Mn are 2+ and 4+, respectively, usually has approximately 10% site exchange between Li and divalent Ni in the Li layer [13]. Thus, the increment of divalent Ni in the Li layer with increasing Mn content is understandable.

Fig. 2 shows SEM images of the synthesized $Li[Ni_{0.52}Co_{0.16+x}Mn_{0.32-x}]O_2$ powders (x = 0–0.16) after the thermal lithiation reaction at 820 °C for 15 h in air. The $Li[Ni_{0.52}Co_{0.16+x}Mn_{0.32-x}]O_2$ powders calcined following the optimum synthetic conditions resulted in dense and spherical particles with an average particle diameter of about 10 μm. The particle diameter of the $Li[Ni_{0.52}Co_{0.16+x}Mn_{0.32-x}]O_2$ powders is similar to the hydroxides, $[Ni_{0.52}Co_{0.16+x}Mn_{0.32-x}](OH)_2$. However, the thread-type primary particle of the hydroxide was completely changed to a rectangular primary particle.

Fig. 3a and b shows the first charge–discharge curves at a current density of 37 mA g^{-1} (0.2 C) and continuous cycling results of the Li/$Li[Ni_{0.52}Co_{0.16+x}Mn_{0.32-x}]O_2$ powders (x = 0–0.16) cells measured in the range of 2.7–4.5 V at a current density of 93 mA g^{-1} (0.5 C) at 25 °C, respectively. It is interesting to note that although the tetravalent Mn content, which is electrochemically inactive, increased, the resulting capacities were similar for all electrodes. It is thought that the content of Mn is likely to affect the oxidation state of Ni. In other words, a lower Mn content may induce the Ni valence to be higher, close to 3+, similar to $Li[Ni_{0.8}Co_{0.1}Mn_{0.1}]O_2$. Meanwhile, the higher concentration of Mn in the $Li[Ni_{0.52}Co_{0.16}Mn_{0.32}]O_2$

Table 1
Rietveld refinement results of XRD data of $Li[Ni_{0.52}Co_{0.16}Mn_{0.32}]O_2$.

Formula: $Li[Ni_{0.52}Co_{0.16}Mn_{0.32}]O_2$
Crystal system: rhombohedral
Space group: $R\bar{3}m$

Atom	Site	*x*	*y*	*z*	*g*	B/Å^2
Li1	3a	0	0	1/2	0.967	0.3
Ni2	3a	0	0	1/2	0.033(2)	0.3
Li2	3b	0	0	0	0.033(2)	0.6
Ni1	3b	0	0	0	0.487	0.6
Mn	3b	0	0	0	0.32	0.6
Co	3b	0	0	0	0.16	0.6
O	6c	0	0	0.258(2)	1	0.8
R_{wp} (%)				9.63		
R_p (%)				10.6		

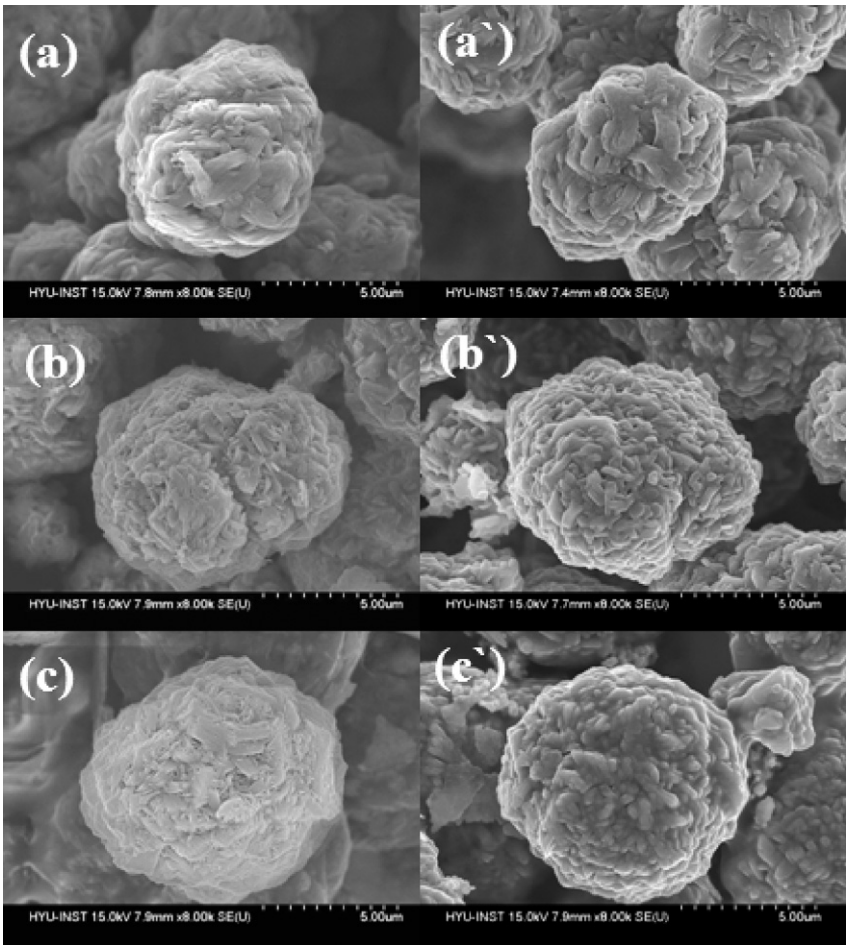

Fig. 2. SEM images of as-coprecipitated $[Ni_{0.52}Co_{0.16+x}Mn_{0.32-x}](OH)_2$ hydroxides; (a) $x = 0$, (b) $x = 0.08$ and (c) $x = 0.16$ and as-synthesized $Li[Ni_{0.52}Co_{0.16+x}Mn_{0.32-x}]O_2$ powders; (a′) $x = 0$, (b′) $x = 0.08$ and (c′) $x = 0.16$.

would tend to lower the Ni valence to close to 2+ as in $Li[Ni_{0.5}Mn_{0.5}]O_2$ or $Li[Ni_{1/3}Co_{1/3}Mn_{1/3}]O_2$. One noticeable difference is the increment of the operation voltage by further incorporation of Mn. The phenomenon is also confirmed when the operation voltages of $Li[Ni_{0.5}Mn_{0.5}]O_2$ and $Li[Ni_{1/3}Co_{1/3}Mn_{1/3}]O_2$ are compared where $Li[Ni_{0.5}Mn_{0.5}]O_2$, which contained more of the electrochemically inactive tetravalent Mn^{4+}, always exhibited a higher operation voltage. Although the details are not known at the present time, a similar effect was found for $Li[Ni_{0.52}Co_{0.16}Mn_{0.32}]O_2$.

Table 2
Structural parameter of $Li[Ni_{0.52}Co_{0.32}Mn_{0.16}]O_2$, $Li[Ni_{0.52}Co_{0.24}Mn_{0.24}]O_2$, and $Li[Ni_{0.52}Co_{0.16}Mn_{0.32}]O_2$ obtained from the refinement results of XRD data.

Composition	a (Å)	c (Å)	Ni^{2+} in Li layer (%)	Rwp (%)
$Li[Ni_{0.52}Co_{0.32}Mn_{0.16}]O_2$	2.8692(2)	14.2388(9)	1.4	9.53
$Li[Ni_{0.52}Co_{0.24}Mn_{0.24}]O_2$	2.8630(1)	14.2172(6)	2.2	12.7
$Li[Ni_{0.52}Co_{0.16}Mn_{0.32}]O_2$	2.8566(2)	14.1879(9)	3.3	9.63

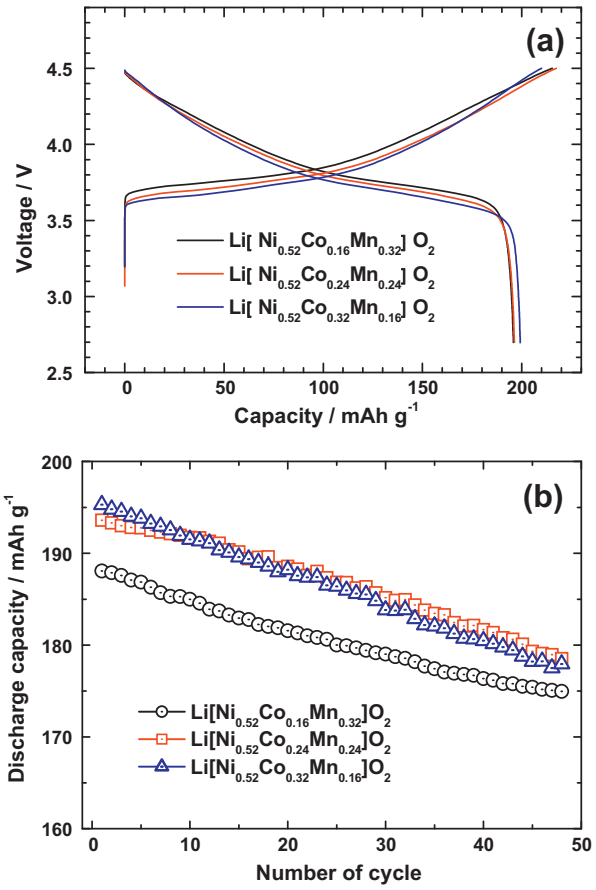

Fig. 3. (a) The initial charge and discharge curves of the $Li[Ni_{0.52}Co_{0.16+x}Mn_{0.32-x}]O_2$ cells at a current density of 37 mA g^{-1} (0.2 C) and (b) cyclability at a current density of 93 mA g^{-1} (0.5 C) in the range of 2.7–4.5 V at 25 °C.

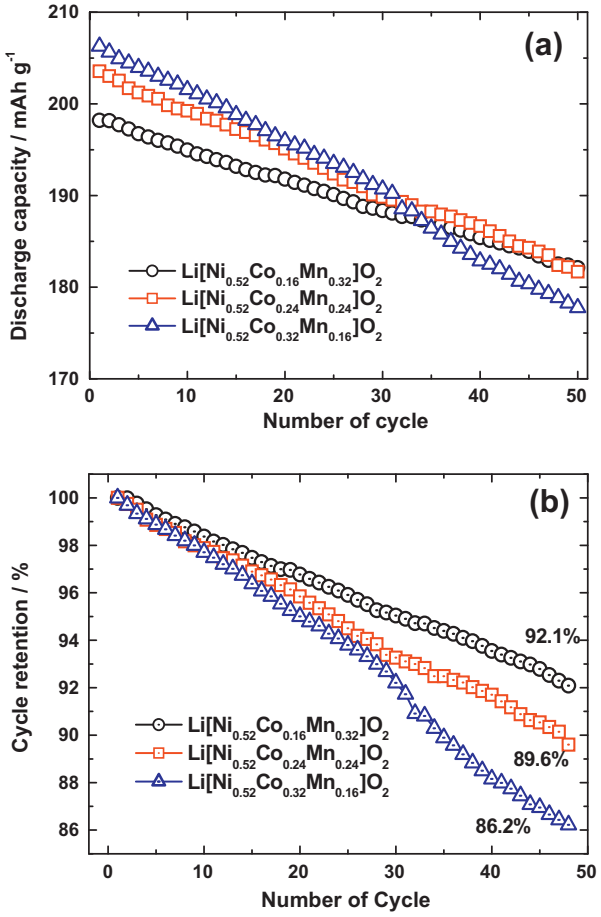

Fig. 4. (a) Cyclability and (b) cycle retention over 50 cycles. The applied current density was 93 mA g^{-1} (0.5 C) in the range of 2.7–4.5 V at 55 °C.

Fig. 4 shows continuous cycling results of the $Li/Li[Ni_{0.52}Co_{0.16+x}Mn_{0.32-x}]O_2$ powders ($x = 0$–0.16) cells between 2.7 and 4.5 V at a current level of 93 mA g^{-1} (0.5 C) at 55 °C. All cells exhibited good cycling performance of more than 90% of initial capacity in the tested voltage range at 25 °C. Meanwhile, for $x = 0$ in $Li[Ni_{0.52}Co_{0.16+x}Mn_{0.32-x}]O_2$, the cell cycled at 55 °C in the same voltage range showed a relatively higher capacity retention of ~92% of its initial capacity, as seen in Fig. 4a. Capacity fading became severe upon cycling with increasing Co content. The capacity retentions for the samples at the 50th cycle are $Li[Ni_{0.52}Co_{0.16}Mn_{0.32}]O_2$ (92.1%) > $Li[Ni_{0.52}Co_{0.24}Mn_{0.24}]O_2$ (89.6%) > $Li[Ni_{0.52}Co_{0.32}Mn_{0.16}]O_2$ (86.2%), as seen in Fig. 4b. Indeed, it was expected that $Li[Ni_{0.52}Co_{0.32}Mn_{0.16}]O_2$ would demonstrate the highest capacity retention because the occupation of divalent Ni in the Li layer was the lowest among the samples, which indicates that Li^+ diffusion may be less disturbed by the presence of Ni in the Li layer. Nonetheless, the best capacity retention was achieved with $Li[Ni_{0.52}Co_{0.16}Mn_{0.32}]O_2$, which had the highest degree of cation mixing in the Li layer. It is known that the electrochemically inactive tetravalent Mn retains the structure during repetitive electrochemical cycling. Thus, the enhanced cycle performance is probably attributed to the presence of a higher content of Mn^{4+}, which provides significant structural stability during cycling [7,10,14].

At the same time, the ac impedance was measured to track the differences of the interfacial resistance with increasing Mn content, as shown in Fig. 5. According to our previous equivalent circuit concerning EIS [15], the high-to-medium frequency semicircle is attributed to resistance of the surface film covering the cathode particles, and the low-frequency one reflects the charge transfer resistance coupled with a double-layer capacitance. After the first cycling, the charge transfer resistances for all electrodes were similar. As cycling continued, the resulting resistances for all electrodes obviously increased as the Mn content decreased. A greater amount of Mn substitution gave rise to a significant decrease in the charge transfer resistance relative to $Li[Ni_{0.52}Co_{0.24}Mn_{0.24}]O_2$ and $Li[Ni_{0.52}Co_{0.32}Mn_{0.16}]O_2$. It is also believed that the Mn^{4+} incorporation into the structure would consequently affect the smaller charge transfer resistance. The reduced increase in the resistance is ascribed to the structural stabilization achieved by introduction of Mn^{4+} in the Co^{3+} sites of $Li[Ni_{0.52}Co_{0.16+x}Mn_{0.32-x}]O_2$.

Fig. 6 shows a comparison of the variation of the lattice parameters of the $Li[Ni_{0.52}Co_{0.16+x}Mn_{0.32-x}]O_2$ ($x = 0$–0.16) electrodes before and after cycling at 55 °C. For $Li[Ni_{0.52}Co_{0.16}Mn_{0.32}]O_2$, there appeared to be slight variation in the lattice parameters before and after cycling. The difference widened in $Li[Ni_{0.52}Co_{0.24}Mn_{0.24}]O_2$ and $Li[Ni_{0.52}Co_{0.32}Mn_{0.16}]O_2$, of which the Mn contents are less than that in $Li[Ni_{0.52}Co_{0.16}Mn_{0.32}]O_2$. This result indicates that the higher Mn concentration was very effective to maintain the layer structure upon cycling. The ex situ XRD studies clearly indicate that the higher Mn content decreased the structural damage during cycling, which eventually led to suppression of the capacity fading. For this reason, the reduced increase in the charge transfer resistance of $Li[Ni_{0.52}Co_{0.16}Mn_{0.32}]O_2$ observed in Fig. 6 is understandable.

Fig. 7 shows the DSC profiles of delithiated $Li_{1-\delta}[Ni_{0.52}Co_{0.16+x}Mn_{0.32-x}]O_2$ ($x = 0$–0.16) charged to 4.5 V. The

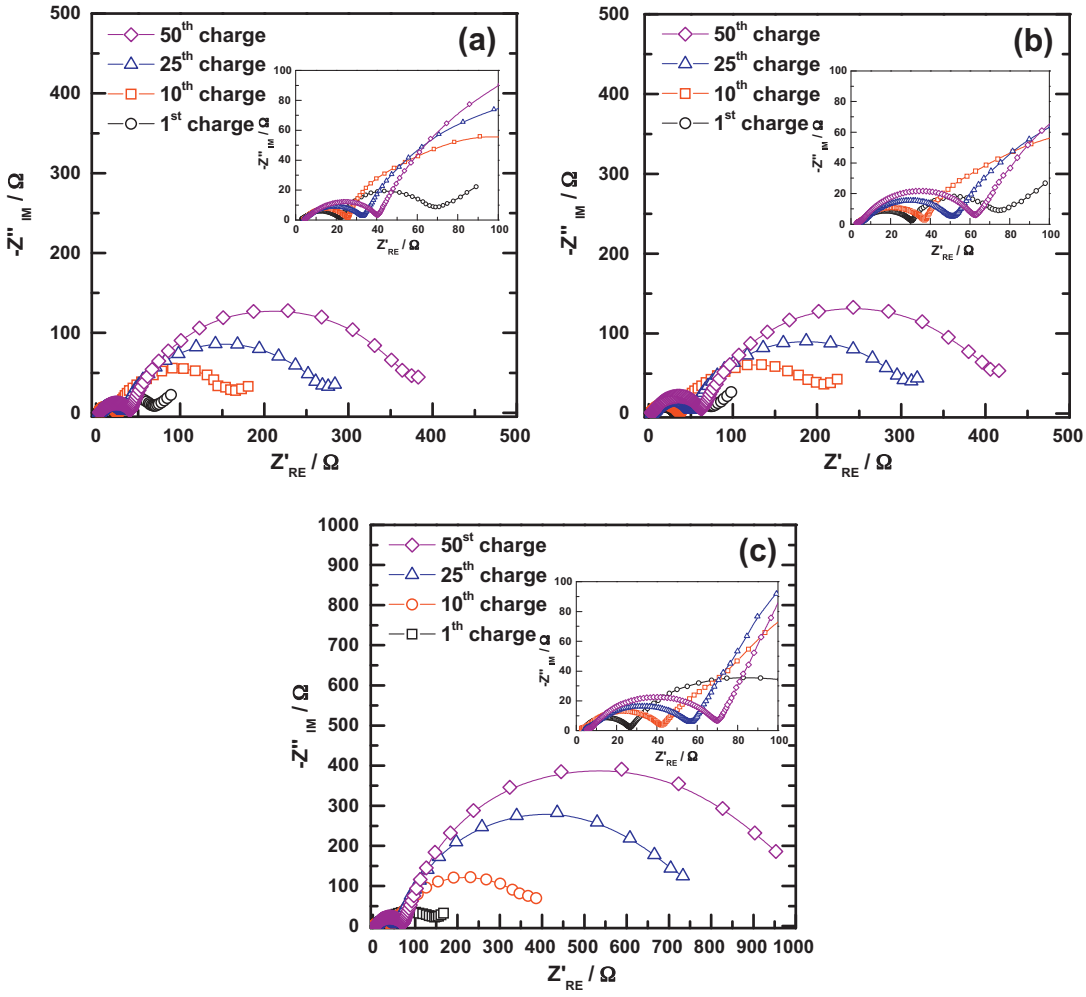

Fig. 5. Nyquist plots of the (a) Li/Li[$Ni_{0.52}Co_{0.16}Mn_{0.32}$]$O_2$, (b) Li/Li[$Ni_{0.52}Co_{0.24}Mn_{0.24}$]$O_2$, and (c) Li/Li[$Ni_{0.52}Co_{0.32}Mn_{0.16}$]$O_2$ cells in the charged state of 4.5 V.

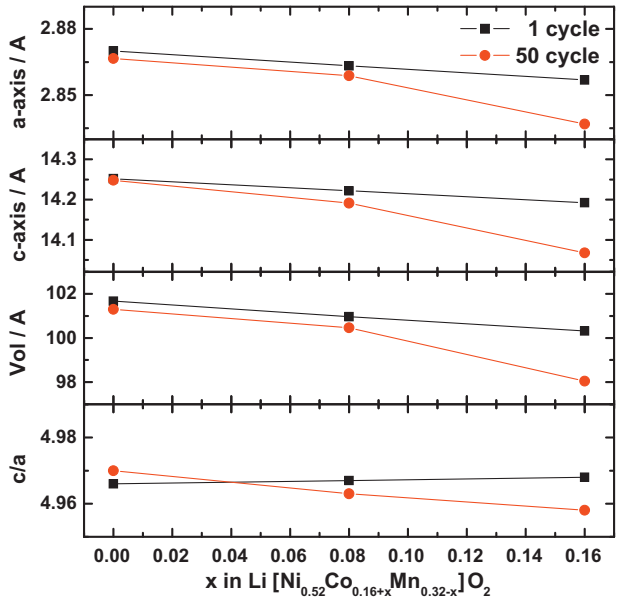

Fig. 6. Variation of lattice parameters (a, c, and c/a) and unit cell volume as a function of Mn content (x) in Li[$Ni_{0.52}Co_{0.16+x}Mn_{0.32-x}$]$O_2$.

onset temperature of the major peak temperature and exothermic heat gerneration of $Li_{1-\delta}[Ni_{0.52}Co_{0.16}Mn_{0.32}]O_2$ were 288.9 °C and 439.1 J g^{-1}, respectively. The onset temperature of the major exothermic reaction gradually shifted to a lower temperature with a higher exothermic heat generation as the Mn content was decreased. This behavior is due to the electrochemically inactive amount of Mn^{4+}, which leads to not only good electrochemical

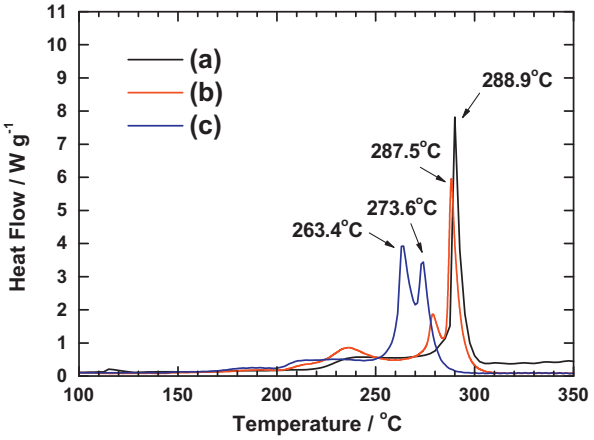

Fig. 7. DSC results of the (a) Li[$Ni_{0.52}Co_{0.16}Mn_{0.32}$]$O_2$, (b) Li[$Ni_{0.52}Co_{0.24}Mn_{0.24}$]$O_2$, and (c) Li[$Ni_{0.52}Co_{0.32}Mn_{0.16}$]$O_2$ cells in the charged state of 4.5 V.

properties but also improved thermal stability in the oxide matrix at a highly delithiated state.

4. Conclusions

In an attempt to understand the effects of the Mn and Co contents on $Li[Ni_{0.52}Co_{0.16+x}Mn_{0.32-x}]O_2$ (x = 0–0.16), we investigated the electrochemical properties and thermal stability of $Li[Ni_{0.52}Co_{0.16+x}Mn_{0.32-x}]O_2$ synthesized via co-precipitation. Rietveld refinement results indicated that the final products had hexagonal α-$NaFeO_2$ structures with a space group of $R\bar{3}m$ and the lattice parameters linearly decreased with increasing Co content. The improved structural and thermal properties caused the enhancement of the specific discharge capacity and cycle life. When designing a positive electrode material for lithium ion batteries with high performance using $Li[Ni_{0.52}Co_{0.16+x}Mn_{0.32-x}]O_2$-type material in the metal composition range of x = 0, 0.08, 0.16, the metal composition, especially $Li[Ni_{0.52}Co_{0.16}Mn_{0.32}]O_2$ which possesses a larger amount of electrochemically inactive Mn^{4+}, is significant in terms of electrochemical stability, cycle life, and thermal stability.

Acknowledgements

This work was supported by the National Research Foundation of Korea (NRF) grant funded by the Korea government (MEST) (no. 2009-0092780). This work was also supported by the Korea Science and Engineering Foundation (KOSEF) grant funded from the Ministry of Education, Science and Technology (MEST) of Korea for the Center for Next Generation Dye-sensitized Solar Cells (no. 2009-0063371).

References

[1] G.G. Amatucci, J.M. Tarascon, L.C. Klein, Solid State Ionics 83 (1996) 1667.
[2] S.-T. Myung, N. Kumagai, S. Komaba, H.-T. Chung, Solid State Ionics 139 (2001) 47.
[3] Z. Liu, A. Yu, J.Y. Lee, J. Power Sources 81–82 (1999) 416.
[4] M. Yoshio, H. Noguchi, J. Itoh, M. Okada, T. Mouri, J. Power Sources 90 (2000) 176.
[5] J.T. Son, E.J. Cairns, Electrochem. Solid-State Lett. 9 (2006) A27.
[6] M.-H. Kim, H.-S. Shin, D. Shin, Y.-K. Sun, J. Power Sources 159 (2006) 1328.
[7] K.S. Lee, S.-T. Myung, K. Amine, Y.-K. Sun, J. Electrochem. Soc. 154 (2007) A971.
[8] M.-H. Lee, Y.-J. Kang, S.-T. Myung, Y.-K. Sun, Electrochim. Acta 50 (2004) 939.
[9] T. Roisnel, J. Rodriguez-Carjaval, Fullprof Manual, Institut Laue-Langevin, Grenoble, France, 2002.
[10] H.-J. Bang, D.-H. Kim, Y.-C. Bae, J. Prakash, Y.-K. Sun, J. Electrochem. Soc. 155 (2008) A95.
[11] S.-T. Myung, N. Kumagai, S. KoMaba, H.-T. Chung, Solid State Ionics 139 (2001) 47.
[12] R.D. Shannon, Acta Crystallogr. A 32 (1976) 751.
[13] K.-S. Lee, S.-T. Myung, J-S. Moon, Y.-K. Sun, Electrochim. Acta 53 (2008) 6033.
[14] Y.-K. Sun, S.-T. Myung, H.-J. Bang, B.-C. Park, S.-J. Park, N.-Y. Sung, J. Electrochem. Soc. 154 (2007) A937.
[15] Y.-K. Sun, S.-T. Myung, C.S. Yoon, D.-W. Kim, Electrochem. Solid-State Lett. 12 (2009) A163.